

PREPARED FOR SUBMISSION TO JHEP

Cross section measurements of the processes $e^+e^- \rightarrow \omega\pi^0$ and $\omega\eta$ at center-of-mass energies between 3.773 and 4.701 GeV

The BESIII collaboration



E-mail: besiii-publications@ihep.ac.cn

ABSTRACT:

The Born cross sections of the processes $e^+e^- \rightarrow \omega\pi^0$ and $e^+e^- \rightarrow \omega\eta$ are measured at center-of-mass energies between 3.773 and 4.701 GeV using a total integrated luminosity of 22.7 fb^{-1} collected with the BESIII detector operating at the BEPCII collider. A simple s^{-n} dependence for the continuum process can describe the measured Born cross sections. No significant contributions from the $\psi(4160)$, $Y(4230)$, $Y(4360)$, $\psi(4415)$, $Y(4660)$ resonances are found.

KEYWORDS: Charmonium(-like), Cross section, BESIII

Contents

1	Introduction	1
2	BESIII detector and Monte Carlo simulation	2
3	Event selection	3
4	Born cross section measurement	3
4.1	$e^+e^- \rightarrow \omega\pi^0$	3
4.2	$e^+e^- \rightarrow \omega\eta$	6
5	Systematic uncertainty	9
6	Summary	11
	The BESIII collaboration	14

1 Introduction

The recent discovery of several charmonium-like (XYZ) states above the open-charm thresholds has attracted great experimental and theoretical interest [1]. Due to the unexpected resonance parameters and decay patterns, they can not be described by conventional quark models, and are considered to be candidates for exotic states, such as hybrids, tetraquarks, and molecules [2–4].

Since 2003, a series of charmonium-like states, such as $X(3872)$ [5], $Y(4260)$ [6] and $Z_c(3900)$ [7, 8], has been discovered. In particular, the vector charmonium-like state $Y(4260)$ was observed by the BaBar experiment in $e^+e^- \rightarrow \gamma_{ISR}\pi^+\pi^-J/\psi$ and confirmed by the CLEO and Belle experiments [9, 10]. In addition, the $Y(4360)$ and $Y(4660)$ were also observed in $e^+e^- \rightarrow \gamma_{ISR}\pi^+\pi^-\psi(3686)$ [11, 12]. Later, the BESIII experiment performed a dedicated scan for the channel $e^+e^- \rightarrow \pi^+\pi^-J/\psi$, revealing that the state previously identified as the $Y(4260)$ consists instead of two structures. The main component, with a mass of $M = (4222.0 \pm 3.1 \pm 1.4) \text{ MeV}/c^2$ [13], was renamed as the $Y(4230)$ by the Particle Data Group (PDG) [1]. The second structure is consistent with the previously observed $Y(4360)$. The $Y(4230)$ is also observed in the processes $e^+e^- \rightarrow \omega\chi_{c0}$ [14], $\pi^+\pi^-h_c$ [15], $\pi^+\pi^-\psi(3686)$ [16], and $\pi^+D^0D^{*-}$ [17]. Experimentally, the Y states were mostly observed in channels with hidden or open charm states. Searches for the Y states decaying into light hadron final states will improve our understanding of the Y states. Several processes with light hadron final states have been measured by the BESIII experiment, such as $e^+e^- \rightarrow K_S^0K^\pm\pi^\mp\pi^0$ and $K_S^0K^\pm\pi^\mp\eta$ [18], $p\bar{n}K_S^0K^- + c.c.$ [19], $p\bar{p}\pi^0$ [20], $p\bar{p}\eta$ and $p\bar{p}\omega$ [21],

etc., but no significant charmonium-like structures are found. Further exploration of other light hadron final states is desirable to probe the nature of the charmonium-like states.

In this paper, we report measurements of the Born cross sections for the $e^+e^- \rightarrow \omega\pi^0$ and $\omega\eta$ processes at center-of-mass energies (\sqrt{s}) between 3.773 and 4.701 GeV with a total integrated luminosity of 22.7 fb^{-1} and the subsequent search for Y states or conventional charmonium states above the continuum contribution.

2 BESIII detector and Monte Carlo simulation

The BESIII detector is a magnetic spectrometer [22] located at the Beijing Electron Positron Collider (BEPCII) [23]. The cylindrical core of the BESIII detector consists of a helium-based multilayer drift chamber (MDC), a plastic scintillator time-of-flight system (TOF), and a CsI (Tl) electromagnetic calorimeter (EMC), which are all enclosed in a superconducting solenoidal magnet, providing a 1.0 T magnetic field. The solenoid is supported by an octagonal flux-return yoke with resistive plate chamber muon identifier modules interleaved with steel. The acceptance of charged particles and photons is 93% over the 4π solid angle. The charged-particle momentum resolution at 1 GeV/ c is 0.5%, and the dE/dx resolution is 6% for the electrons from Bhabha scattering. The EMC measures photon energies with a resolution of 2.5% (5%) at 1 GeV in the barrel (end cap) region. The time resolution of the TOF barrel section is 68 ps, while that of the end cap section is 110 ps. The end cap TOF system was upgraded in 2015 with multi-gap resistive plate chamber technology, providing a time resolution of 60 ps [24]; this improvement benefits 25 of the 34 energy points used in this paper.

Simulated data samples produced with the GEANT4-based [25] Monte Carlo (MC) package, which includes the geometric description of the BESIII detector and the detector response, are used to determine the detection efficiency and to estimate the background contributions. The simulation includes the beam energy spread and initial-state radiation (ISR) in the e^+e^- annihilations modeled with the generator KKMC [26]. The ISR production of vector charmonium(-like) states and the continuum processes are incorporated also in KKMC [26]. The known decay modes are modeled with EVTGEN [27], using branching fractions summarized and averaged by the PDG [1], and the remaining unknown decays from the charmonium states are generated with LUNDCHARM [28]. Final state radiation from charged final state particles is incorporated with the PHOTOS package [29].

Signal MC samples for $e^+e^- \rightarrow \omega\pi^0$ and $\omega\eta$ are generated using HELAMP (helicity amplitude model) and EVTGEN [27] at each center-of-mass energy point. The event selection criteria and the detection efficiencies are determined and studied based on signal MC samples of 1×10^5 signal events generated for each value of \sqrt{s} . Detection efficiencies are determined by the ratio of the reconstructed event yields (after the selection criteria) to the number of the generated events.

3 Event selection

For each charged track, the distance of closest approach to the interaction point (IP) is required to be within 10 cm in the beam direction and within 1 cm in the plane perpendicular to the beam direction. The polar angles (θ) of the tracks must be within the fiducial volume of the MDC, $|\cos \theta| < 0.93$. Photons are reconstructed from isolated showers in the EMC, which are at least 10° away from the nearest charged track. The photon energy is required to be at least 25 MeV in the barrel region ($|\cos \theta| < 0.80$) or 50 MeV in the end cap region ($0.86 < |\cos \theta| < 0.92$). To suppress electronic noise and energy depositions unrelated to the event, the EMC cluster timing from the reconstructed event start time is further required to satisfy $0 \leq t \leq 700$ ns.

The final state ω is reconstructed via $\omega \rightarrow \pi^+\pi^-\pi^0$; this π^0 is referred to as the resonance π^0 . In addition there is a “bachelor” π^0 (η). All π^0 and η are reconstructed via the decays to $\gamma\gamma$. Given this topology, candidate events are required to have two charged tracks with zero net charge and at least four photons. The flight time in the TOF and dE/dx information in the MDC are combined to calculate particle identification (PID) likelihoods for the π , K , and p hypotheses. For both charged tracks, it is required that the likelihood for a pion assignment is larger than that for both the kaon and proton hypotheses.

A six-constraint (6C) kinematic fit is performed to the candidate events with $e^+e^- \rightarrow \pi^+\pi^-\pi^0\pi^0, \pi^+\pi^-\pi^0\eta$ hypothesis. The total four-momentum is constrained to the initial four-momentum of the e^+e^- system. The invariant mass of two photons from the ω resonance π^0 decay is constrained to the nominal π^0 mass [1] and the other two photons, from the bachelor π^0 (η) decay, are constrained to the nominal masses of the π^0 (η) [1]. Multiple combinations arise from different photon pairings as well as events with more than four photon candidates. The combination with the smallest χ_{6C}^2 is chosen. For the two π^0 candidates in $e^+e^- \rightarrow \omega\pi^0$, the momentum of the bachelor π^0 is larger than that of the π^0 from ω decay at all the energy points, allowing for separation of the π^0 candidates. Figure 1 (a) shows the momentum distributions of π^0 at $\sqrt{s} = 3.773$ GeV for the signal MC.

In order to study the non-resonant backgrounds, a five-constraint (5C) kinematic fit is performed on the selected candidate events. This fit is simply the 6C kinematic fit with the mass constraint on the bachelor π^0 (η) removed. The χ_{5C}^2 is required to be less than 60; further details are given in the next section. According to a study of inclusive MC samples with an event-type investigation tool, TopoAna [30], the main background for $e^+e^- \rightarrow \omega\eta$ is the ISR process $e^+e^- \rightarrow \omega\gamma_{ISR}$. To remove the background, the angle between the two photons from the η in the laboratory frame, $\theta_{\gamma\gamma}$, is required to be less than 1 radian. Figure 1 (b) shows the distribution of $\theta_{\gamma\gamma}$ at $\sqrt{s} = 3.773$ GeV.

4 Born cross section measurement

4.1 $e^+e^- \rightarrow \omega\pi^0$

Figure 2 (a) shows the distribution of $M(\pi^+\pi^-\pi^0)$ versus $M(\gamma\gamma)$ for data at $\sqrt{s} = 3.773$ GeV. Here, $M(\gamma\gamma)$ is the invariant mass of the two photons from the bachelor π^0 decay. A clear $\omega\pi^0$ signal can be seen. Figure 2 (b) shows the distribution of $M(\pi^+\pi^-\pi^0)$ for data

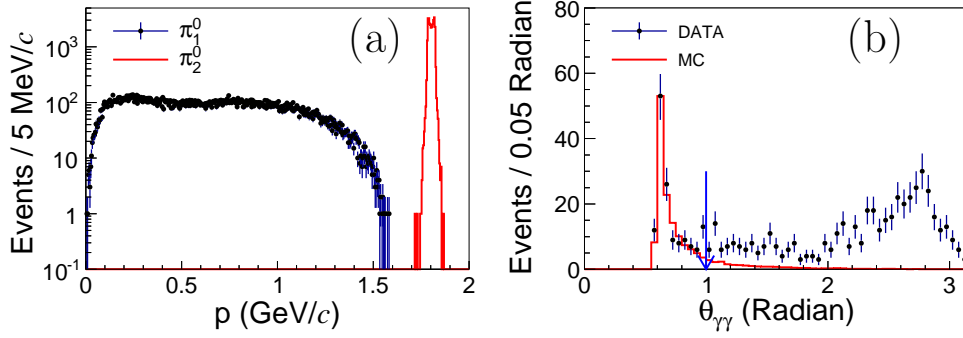


Figure 1. (a) Momentum distributions of the π^0 from signal MC in the lab-frame at $\sqrt{s} = 3.773$ GeV for $e^+e^- \rightarrow \omega\pi^0$. Here, π_1^0 is from ω resonance, and π_2^0 is the bachelor, directly from e^+e^- . (b) The distribution of $\theta_{\gamma\gamma}$ for the $\eta \rightarrow \gamma\gamma$ at $\sqrt{s} = 3.773$ GeV for $e^+e^- \rightarrow \omega\eta$. Dots with error bars are data, the red solid line is signal MC, the vertical blue arrow indicates the requirement, $\theta_{\gamma\gamma} < 1.0$ radian, that is used to select signal events.

at $\sqrt{s} = 3.773$ GeV. In the fit, the ω signal is described by a double Gaussian function, plus a linear background function. Based on signal MC simulation, the ω signal region is defined as the mass range $[0.7500, 0.8150]$ GeV/ c^2 in $M(\pi^+\pi^-\pi^0)$, and is indicated by the horizontal dashed lines in Figure 2 (a). The sideband regions, defined as the range $[0.6525, 0.7175] \cup [0.8475, 0.9125]$ GeV/ c^2 as indicated by the solid arrows in Figure 2 (b), are used to study the non- ω background.

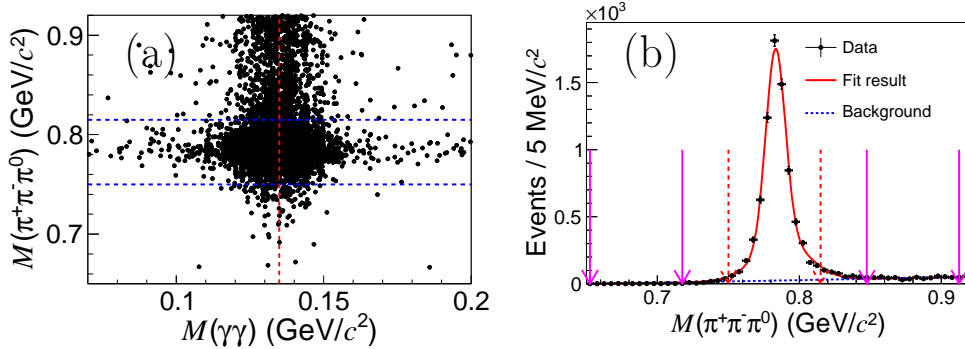


Figure 2. (a) $M(\pi^+\pi^-\pi^0)$ versus $M(\gamma\gamma)$ for data at $\sqrt{s} = 3.773$ GeV. The blue dashed lines mark the signal band of the ω , and the red dashed line marks the mass of the π^0 . (b) Fit to distribution of $M(\pi^+\pi^-\pi^0)$ for the events in (a). The red dashed arrows mark the signal region of the ω , and the pink solid arrows mark the sideband regions of the ω .

Figure 3 shows the distributions of $M(\gamma\gamma)$ from the signal region (a) and the sideband region (b) of the ω for data at $\sqrt{s} = 3.773$ GeV. To account for non- ω backgrounds, the signal yields are obtained by unbinned maximum likelihood fits to the π^0 signal in the $M(\gamma\gamma)$ spectrum for events in the ω signal and sideband regions. The signal function comes from the MC-simulated shape, while the background shape is described by a linear background function. The fit results are shown in Figure 3. The net number of signal events

is calculated by $N^{\text{sig}} = N^{\text{obs}} - N^{\text{bkg}} \cdot f_{\text{scale}}$, where N^{obs} and N^{bkg} are the number of π^0 events in the ω signal and sideband regions, respectively; $f_{\text{scale}} = 0.5$ is the ratio between the signal and sideband region widths.

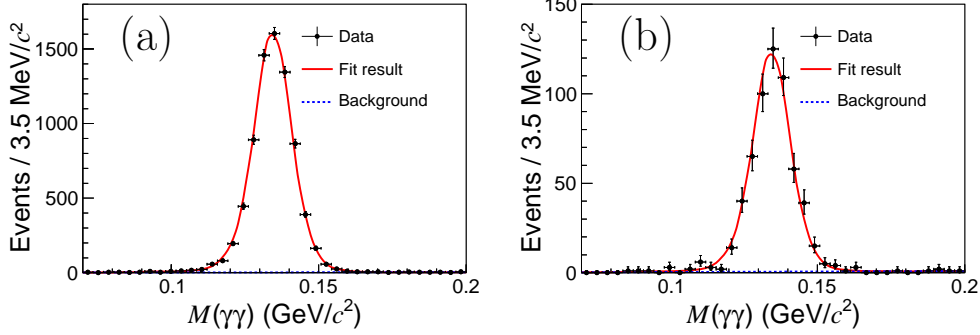


Figure 3. Fits to the distributions of $M(\gamma\gamma)$ for data from the ω signal region (a) and the ω sideband region (b) at $\sqrt{s} = 3.773$ GeV.

The Born cross section for $e^+e^- \rightarrow \omega\pi^0$ is calculated using the following formula:

$$\sigma^{\text{Born}}(\sqrt{s}) = \frac{N^{\text{sig}}}{\mathcal{L} \cdot \epsilon \cdot \mathcal{B} \cdot (1 + \delta(s)) \cdot \frac{1}{|1 - \Pi|^2}}, \quad (4.1)$$

where N^{sig} is the number of signal events, \mathcal{L} is the integrated luminosity, ϵ is the detection efficiency, \mathcal{B} is the product of the branching fractions in the full decay chain, $\mathcal{B} = \mathcal{B}(\omega \rightarrow \pi^+\pi^-\pi^0) \cdot \mathcal{B}^2(\pi^0 \rightarrow \gamma\gamma) \approx 87.21\%$ taken from the PDG [1], $(1 + \delta(s))$ and $\frac{1}{|1 - \Pi|^2}$ are factors for the ISR correction and vacuum polarization, respectively. To obtain the ISR factor, we take the initial line shape of the observed cross section as an energy-dependent function $a \cdot s^{-n}$, which is used to describe the continuum process, and obtain the Born cross section iteratively until the results become stable within 1% at all energies. The relevant numbers related to the Born cross section measurement are listed in Table 1. Figure 4 shows the energy-dependent Born cross section for $e^+e^- \rightarrow \omega\pi^0$, where $n = 3.51 \pm 0.05$, and the goodness of fit is $\chi^2/n.d.f. = 33.00/32$, where $n.d.f.$ is the number of degrees of freedom.

The potential contribution from conventional charmonium or charmonium-like states, $\psi(4160)$, $Y(4230)$, $Y(4360)$, $\psi(4415)$, and $Y(4660)$, is investigated by fitting the dressed cross section using the coherent sum of the continuum and an additional charmonium(-like) state amplitude. The corresponding fit function [31] is expressed as

$$\sigma^{\text{D}}(\sqrt{s}) = \left| \left(a \cdot s^{-n} \right)^{1/2} + \frac{\sqrt{12\pi\Gamma_{ee}\mathcal{B}(\omega\pi^0)\Gamma}}{s - M^2 + iM\Gamma} \left(\frac{PS(\sqrt{s})}{PS(M)} \right)^{3/2} e^{i\phi} \right|^2, \quad (4.2)$$

where $\sigma^{\text{D}}(\sqrt{s}) = \sigma^{\text{Born}}(\sqrt{s})/|1 - \Pi|^2$, is the dressed cross section, ϕ is the phase angle between the amplitude of the continuum process and the charmonium(-like) state, $PS(\sqrt{s})$ is the two-body phase space factor, Γ_{ee} is the e^+e^- partial width, $\mathcal{B}(\omega\pi^0)$ is the branching fraction of charmonium(-like) decays to $\omega\pi^0$ final state, M and Γ are the mass and width of charmonium(-like) state, which are fixed to their nominal values [1].

Table 1. The Born cross sections for $e^+e^- \rightarrow \omega\pi^0$ and $\omega\eta$, together with integrated luminosities \mathcal{L}_{int} , number of signal events N^{sig} , ISR factors $1+\delta(s)$, vacuum polarization factors $\frac{1}{|1-\Pi|^2}$, and efficiencies ϵ . Here, σ^{Born} represents $\sigma_{\omega\pi^0}^{\text{Born}}$ or $\sigma_{\omega\eta}^{\text{Born}}$. For N^{sig} and σ^{Born} , errors are statistical only. The first values in brackets are for the process $e^+e^- \rightarrow \omega\pi^0$, and the second for the process $e^+e^- \rightarrow \omega\eta$.

$\sqrt{s}(\text{GeV})$	$\mathcal{L}_{\text{int}}(\text{pb}^{-1})$	N^{sig}	$1 + \delta(s)$	$\frac{1}{ 1-\Pi ^2}$	$\epsilon(\%)$	$\sigma^{\text{Born}}(\text{pb})$
3.773	2931.8	$(7335.2 \pm 88.9, 96.8 \pm 10.6)$	(1.0473, 1.0391)	1.057	(19.38, 15.01)	$(13.37 \pm 0.16, 0.58 \pm 0.06)$
3.867	108.9	$(247.2 \pm 16.4, 4.7^{+2.6}_{-2.0})$	(1.0678, 1.0570)	1.051	(19.02, 15.49)	$(12.21 \pm 0.81, 0.72^{+0.40}_{-0.31})$
3.871	110.3	$(240.4 \pm 16.0, 4.6^{+2.6}_{-2.0})$	(1.0693, 1.0578)	1.051	(18.93, 15.58)	$(11.75 \pm 0.78, 0.69^{+0.39}_{-0.30})$
4.008	482.0	$(779.8 \pm 29.0, 13.2^{+4.5}_{-3.9})$	(1.0983, 1.0853)	1.044	(18.11, 15.43)	$(8.93 \pm 0.33, 0.45^{+0.15}_{-0.13})$
4.129	401.5	$(524.0 \pm 23.7, 11.2^{+4.0}_{-3.4})$	(1.1248, 1.1088)	1.053	(17.69, 14.88)	$(7.14 \pm 0.32, 0.46^{+0.15}_{-0.13})$
4.158	408.7	$(491.6 \pm 23.2, 5.0^{+3.2}_{-2.6})$	(1.1311, 1.1148)	1.054	(17.56, 15.10)	$(6.59 \pm 0.31, 0.20^{+0.13}_{-0.10})$
4.178	3194.5	$(3840.7 \pm 63.8, 59.5 \pm 9.3)$	(1.1352, 1.1190)	1.055	(17.24, 14.97)	$(6.68 \pm 0.11, 0.30 \pm 0.05)$
4.189	526.7	$(649.0 \pm 26.6, 15.8^{+4.6}_{-3.9})$	(1.1386, 1.1207)	1.056	(17.21, 14.84)	$(6.84 \pm 0.28, 0.49^{+0.14}_{-0.12})$
4.199	526.0	$(601.1 \pm 25.5, 13.8^{+4.1}_{-3.5})$	(1.1398, 1.1224)	1.057	(17.24, 14.93)	$(6.31 \pm 0.27, 0.43^{+0.13}_{-0.11})$
4.209	517.1	$(603.9 \pm 25.5, 19.1^{+4.9}_{-4.2})$	(1.1421, 1.1242)	1.057	(16.99, 14.64)	$(6.53 \pm 0.28, 0.61^{+0.16}_{-0.13})$
4.219	514.6	$(555.3 \pm 24.7, 6.7^{+3.1}_{-2.4})$	(1.1439, 1.1257)	1.057	(16.94, 14.83)	$(6.04 \pm 0.27, 0.21^{+0.10}_{-0.08})$
4.226	1056.4	$(1134.3 \pm 34.7, 23.4^{+5.6}_{-4.9})$	(1.1454, 1.1278)	1.057	(17.38, 15.05)	$(5.85 \pm 0.18, 0.35^{+0.08}_{-0.07})$
4.236	530.3	$(624.3 \pm 26.1, 3.7^{+2.6}_{-1.9})$	(1.1488, 1.1296)	1.056	(16.99, 14.77)	$(6.55 \pm 0.27, 0.11^{+0.08}_{-0.06})$
4.244	538.1	$(580.3 \pm 25.2, 11.0^{+4.0}_{-3.3})$	(1.1504, 1.1320)	1.056	(16.94, 14.65)	$(6.01 \pm 0.26, 0.34^{+0.12}_{-0.10})$
4.258	828.4	$(914.5 \pm 31.6, 19.2^{+5.1}_{-4.5})$	(1.1535, 1.1339)	1.054	(16.59, 14.52)	$(6.28 \pm 0.22, 0.38^{+0.10}_{-0.09})$
4.267	531.1	$(537.2 \pm 24.1, 7.0^{+3.2}_{-2.6})$	(1.1561, 1.1359)	1.053	(16.64, 15.06)	$(5.73 \pm 0.26, 0.21^{+0.10}_{-0.08})$
4.278	175.7	$(190.4 \pm 14.3, 3.6^{+2.5}_{-1.8})$	(1.1582, 1.1375)	1.053	(16.82, 14.50)	$(6.06 \pm 0.45, 0.34^{+0.24}_{-0.17})$
4.288	502.4	$(486.1 \pm 22.8, 10.7^{+3.9}_{-3.3})$	(1.1609, 1.1396)	1.053	(16.77, 14.68)	$(5.41 \pm 0.25, 0.35^{+0.13}_{-0.11})$
4.312	501.2	$(494.8 \pm 23.2, 15.8^{+4.5}_{-3.9})$	(1.1662, 1.1453)	1.052	(16.89, 14.69)	$(5.46 \pm 0.26, 0.51^{+0.15}_{-0.13})$
4.338	505.0	$(463.9 \pm 22.4, 5.1^{+3.0}_{-2.4})$	(1.1722, 1.1513)	1.051	(16.58, 14.58)	$(5.16 \pm 0.25, 0.16^{+0.10}_{-0.08})$
4.358	543.9	$(477.1 \pm 22.6, 9.0^{+3.8}_{-3.2})$	(1.1770, 1.1558)	1.051	(16.77, 14.62)	$(4.85 \pm 0.23, 0.27^{+0.11}_{-0.10})$
4.378	522.7	$(420.6 \pm 21.5, 8.4^{+3.8}_{-3.2})$	(1.1819, 1.1591)	1.052	(16.43, 14.49)	$(4.52 \pm 0.23, 0.26^{+0.12}_{-0.10})$
4.397	507.8	$(391.7 \pm 20.5, 10.0^{+3.9}_{-3.2})$	(1.1858, 1.1626)	1.051	(16.34, 14.45)	$(4.34 \pm 0.23, 0.32^{+0.13}_{-0.11})$
4.416	1043.9	$(814.7 \pm 29.7, 13.1^{+4.4}_{-3.8})$	(1.1903, 1.1670)	1.053	(16.38, 14.38)	$(4.36 \pm 0.16, 0.20^{+0.07}_{-0.06})$
4.437	569.9	$(471.9 \pm 22.7, 11.9^{+4.1}_{-3.4})$	(1.1950, 1.1709)	1.054	(16.15, 14.29)	$(4.67 \pm 0.22, 0.34^{+0.12}_{-0.10})$
4.467	111.1	$(70.2 \pm 8.6, 0.3^{+1.6}_{-0.3})$	(1.2029, 1.1773)	1.055	(16.08, 14.27)	$(3.55 \pm 0.43, 0.04^{+0.23}_{-0.04})$
4.527	112.1	$(90.0 \pm 9.6, 0.0^{+1.1}_{-0.0})$	(1.2177, 1.1886)	1.055	(15.87, 14.16)	$(4.51 \pm 0.48, 0.00^{+0.16}_{-0.00})$
4.600	586.9	$(347.3 \pm 19.5, 7.5^{+3.5}_{-2.8})$	(1.2354, 1.2055)	1.055	(15.13, 13.70)	$(3.44 \pm 0.19, 0.21^{+0.10}_{-0.08})$
4.615	102.5	$(51.2 \pm 7.6, 0.0^{+1.2}_{-0.0})$	(1.2386, 1.2087)	1.055	(15.20, 13.63)	$(2.88 \pm 0.43, 0.00^{+0.19}_{-0.00})$
4.630	511.1	$(259.5 \pm 17.1, 3.0^{+2.3}_{-1.6})$	(1.2434, 1.2119)	1.055	(15.04, 13.61)	$(2.95 \pm 0.19, 0.10^{+0.07}_{-0.05})$
4.643	541.4	$(285.4 \pm 17.8, 1.0^{+1.7}_{-1.0})$	(1.2466, 1.2158)	1.055	(15.09, 13.34)	$(3.05 \pm 0.19, 0.03^{+0.05}_{-0.03})$
4.664	523.6	$(273.3 \pm 17.1, 4.5^{+2.9}_{-2.0})$	(1.2522, 1.2191)	1.055	(14.94, 13.75)	$(3.03 \pm 0.19, 0.14^{+0.08}_{-0.06})$
4.684	1631.7	$(814.9 \pm 29.8, 17.5^{+5.2}_{-4.5})$	(1.2569, 1.2226)	1.055	(14.89, 13.53)	$(2.90 \pm 0.11, 0.18^{+0.05}_{-0.05})$
4.701	526.2	$(247.4 \pm 16.5, 7.7^{+3.3}_{-2.7})$	(1.2618, 1.2271)	1.055	(14.65, 13.55)	$(2.76 \pm 0.18, 0.24^{+0.10}_{-0.08})$

To examine the significance of the potential charmonium(-like) state, the fit is repeated using only the continuum amplitude. The significance is calculated taking into account the difference in likelihood value and the change in the number of degrees of freedom from the two fits. Table 2 lists the fit parameters and the significance for additional charmonium(-like) states. No obvious structure is found in the process of $e^+e^- \rightarrow \omega\pi^0$.

4.2 $e^+e^- \rightarrow \omega\eta$

Figure 5 shows the distribution of $M(\pi^+\pi^-\pi^0)$ versus $M(\gamma\gamma)$ (from η) for data at $\sqrt{s} = 3.773$ GeV. Clear $\omega\eta$ signals are observed. The ω signal region is defined as the mass range $[0.7500, 0.8150]$ GeV/ c^2 in $M(\pi^+\pi^-\pi^0)$ and is indicated by the horizontal dashed lines. The

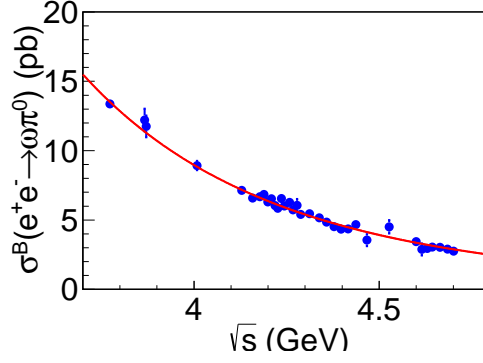


Figure 4. Fit to the Born cross sections of $e^+e^- \rightarrow \omega\pi^0$ with function $a \cdot s^{-n}$.

Table 2. Results of the fits to the dressed cross section $\sigma^D(\sqrt{s})$. “Solution I” represents the constructive solution, and “Solution II” represents the destructive solution. The uncertainty is statistical only.

Channel	Resonance	$\Gamma_{ee} \cdot \mathcal{B}$ (eV) Solution I	$\Gamma_{ee} \cdot \mathcal{B}$ (eV) Solution II	Significance
$\omega\pi^0$	$\psi(4160)$	$(2.31 \pm 2.92) \times 10^{-4}$	2.29 ± 0.02	1.2σ
	$Y(4230)$	$(2.96 \pm 7.61) \times 10^{-5}$	1.39 ± 0.01	0.3σ
	$Y(4360)$	$(5.26 \pm 5.18) \times 10^{-4}$	2.51 ± 0.03	1.5σ
	$\psi(4415)$	$(5.13 \pm 15.21) \times 10^{-5}$	1.54 ± 0.02	0.3σ
	$Y(4660)$	$(3.97 \pm 4.82) \times 10^{-4}$	1.23 ± 0.02	1.2σ
$\omega\eta$	$\psi(4160)$	$(4.33 \pm 7.75) \times 10^{-4}$	$(1.14 \pm 0.07) \times 10^{-1}$	0.8σ
	$Y(4230)$	$(2.41 \pm 4.21) \times 10^{-4}$	$(6.99 \pm 0.52) \times 10^{-2}$	0.6σ
	$Y(4360)$	$(7.82 \pm 13.36) \times 10^{-4}$	$(1.33 \pm 0.14) \times 10^{-1}$	0.7σ
	$\psi(4415)$	$(9.66 \pm 16.16) \times 10^{-4}$	$(7.74 \pm 1.10) \times 10^{-2}$	0.8σ
	$Y(4660)$	$(3.45 \pm 3.22) \times 10^{-3}$	$(5.02 \pm 0.97) \times 10^{-2}$	1.8σ

sideband regions, defined as the range $[0.6525, 0.7175] \cup [0.8475, 0.9125] \text{ GeV}/c^2$, are used to study the non- ω background.

Figure 6 shows the distributions of $M(\gamma\gamma)$ for data at $\sqrt{s} = 3.773 \text{ GeV}$. No obvious non- ω events are seen as indicated by the very small sideband contribution in the green shaded histogram. The yield of signal events is obtained by an unbinned maximum likelihood fit to the η signal in the $M(\gamma\gamma)$ spectrum for events in the ω signal region. The signal function is described by the MC-simulated shape, and the background shape is described by a linear function.

The Born cross section for $e^+e^- \rightarrow \omega\eta$ is calculated using Eq. 4.1, where the N^{sig} is the signal yield for $e^+e^- \rightarrow \omega\eta$, \mathcal{B} is the product of the branching fractions in the full decay chain $\mathcal{B} = \mathcal{B}(\omega \rightarrow \pi^+\pi^-\pi^0) \cdot \mathcal{B}(\pi^0 \rightarrow \gamma\gamma) \cdot \mathcal{B}(\eta \rightarrow \gamma\gamma) \approx 34.78\%$ taken from the PDG [1]. The Born cross section is obtained utilizing same method as described above. Figure 7 shows the energy-dependent Born cross section for $e^+e^- \rightarrow \omega\eta$, where $n = 3.24 \pm 0.44$, and the goodness of fit $\chi^2/n.d.f. = 40.45/32$.

The contribution from charmonium(-like) states $\psi(4160)$, $Y(4230)$, $Y(4360)$, $\psi(4415)$ and $Y(4660)$, is investigated similar as the previous part. The corresponding fit function is defined as Eq. 4.2 in which only $\omega\pi^0$ is replaced by $\omega\eta$. Table 2 lists the fit parameters and

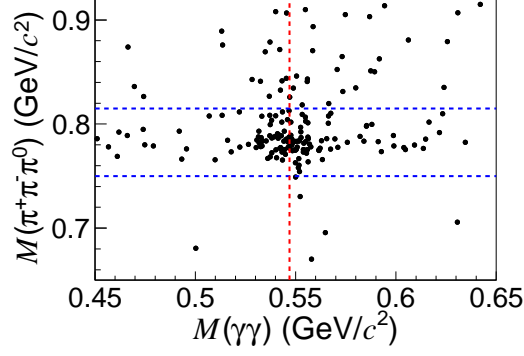


Figure 5. $M(\pi^+\pi^-\pi^0)$ versus $M(\gamma\gamma)$ for data at $\sqrt{s} = 3.773$ GeV for $e^+e^- \rightarrow \omega\eta$. The blue dashed lines mark the signal bands of ω , and the red dashed line mark the known mass of η .

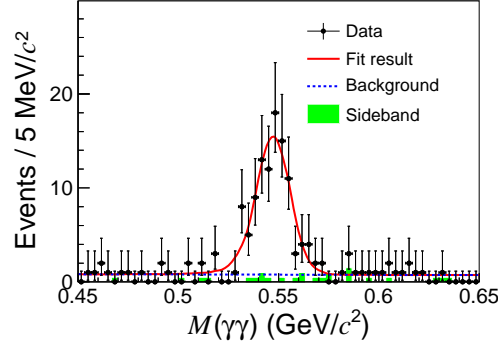


Figure 6. The $M(\gamma\gamma)$ invariant mass distribution for the data at $\sqrt{s} = 3.773$ GeV for $e^+e^- \rightarrow \omega\eta$. The red solid line is the fit to the data and the blue dashed line is the background component. The green shaded histogram corresponds to the normalized background events from the ω sideband region.

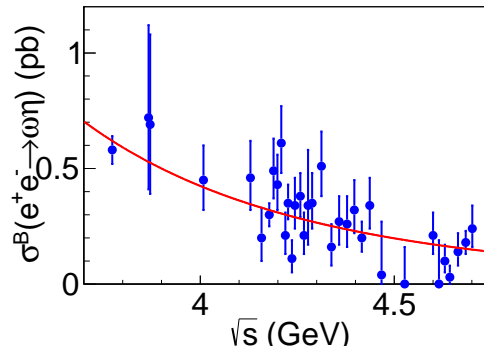


Figure 7. Fit to the Born cross sections of $e^+e^- \rightarrow \omega\eta$ with function $a \cdot s^{-n}$.

the significance for the charmonium(-like) states. No significant charmonium(-like) state is found in the process $e^+e^- \rightarrow \omega\eta$.

5 Systematic uncertainty

The systematic uncertainties in the measurement of $\sigma_{\omega\pi^0}^{\text{Born}}$ and $\sigma_{\omega\eta}^{\text{Born}}$ originate from the luminosity measurement, the tracking efficiency, the photon detection efficiency, the PID efficiency, the kinematic fit, the ω mass window, the fitting procedure, the peaking background, the $\theta_{\gamma\gamma}$ requirement, the ISR correction, and the input branching fractions from intermediate states.

The integrated luminosity at each point has been measured with a precision of 1.0% using the Bhabha process [32].

The uncertainty from the tracking efficiency is determined to be 1.0% per track [33] and the uncertainty in photon detection efficiency is 1.0% per photon [31].

The uncertainty due to PID efficiency is determined to be 1.0% per pion [34].

The uncertainty due to the kinematic fit requirements is estimated by correcting the helix parameters of charged tracks according to the method described in Ref. [35]. The difference between detection efficiencies obtained from MC samples with and without this correction is taken as the uncertainty.

The uncertainty from the ω mass window is estimated by changing the window range by $\pm 10\%$, the maximum difference of final results is taken as systematic uncertainty.

The uncertainty caused by fitting procedure includes the signal shape, background shape and fit range. The original MC-simulated signal shape is replaced by a MC-simulated shape convolved with a Gaussian function, and the difference is taken as the uncertainty from the signal shape. The original linear background function is replaced by a 2nd-order Chebychev polynomial or a constant one, and the maximum difference is taken as the uncertainty from the background shape. The fit range is varied by $\pm 10\%$ at both boundaries, and the maximum difference is taken as the uncertainty from the fit range. The uncertainties from these last three sources are added in quadrature and taken as the total uncertainty from the fitting procedure.

In estimating the systematic uncertainties caused by the ω mass window and fitting procedure for the channel $e^+e^- \rightarrow \omega\eta$, the data in all energies are combined together due to the poor statistics.

The uncertainty caused by the peaking background subtraction for the channel $e^+e^- \rightarrow \omega\pi^0$ includes the ω sideband region and fitting procedure. The ω sideband regions are shifted by ± 6.5 MeV/ c^2 (10% of their widths), and the largest difference of final results is taken as the systematic uncertainty.

The uncertainty due to the $\theta_{\gamma\gamma}$ requirement for the channel $e^+e^- \rightarrow \omega\eta$ is estimated by an alternative analysis without the cut criterion of $\theta_{\gamma\gamma} < 1$ radian, and the difference of final results is taken as the systematic uncertainty. For the data at energies other than 3.773 GeV, the uncertainties are set as those of 3.773 GeV due to the poor statistics.

The uncertainty from ISR correction factor is estimated by changing the power n in function $\sigma(\sqrt{s}) = a \cdot s^{-n}$, which is used to describe the line shapes of $e^+e^- \rightarrow \omega\pi^0, \omega\eta$.

The continuum exponent n is shifted by $\pm 1\sigma$ relative to the nominal value, and the largest difference of the final result is taken as systematic uncertainty.

The uncertainties caused by the branching fractions from intermediate states are taken from the PDG [1].

Table 3 summarizes all the systematic uncertainties related to $\sigma_{\omega\pi^0}^{\text{Born}}$ and $\sigma_{\omega\eta}^{\text{Born}}$ for each center-of-mass energy. The total systematic uncertainty for each energy point is calculated as the quadratic sum of the individual uncertainties, assuming them to be uncorrelated.

Table 3. Summary of relative systematic uncertainties (%) associated with luminosity (\mathcal{L}_{int}), tracking efficiency (Tracks), photon detection efficiency (Photons), PID efficiency (PID), kinematic fit (χ_{5C}^2), ω mass window (ω), fitting procedure (Fit), peaking background (Peaking), $\theta_{\gamma\gamma}$ requirement ($\theta_{\gamma\gamma}$), ISR correction factor (ISR) and branching fraction (\mathcal{B}). The first values in brackets are for the process $e^+e^- \rightarrow \omega\pi^0$, and the second for the process $e^+e^- \rightarrow \omega\eta$. A dash indicates that the systematic uncertainty is not applicable.

\sqrt{s} (GeV)	\mathcal{L}_{int}	Tracks	Photons	PID	χ_{5C}^2	ω	Fit	Peaking	$\theta_{\gamma\gamma}$	ISR	\mathcal{B}	Sum
3.773	1.0	2.0	4.0	2.0	(0.3, 0.3)	(0.3, 1.7)	(0.2, 4.8)	(0.1, -)	(-, 0.5)	(1.5, 1.1)	(0.7, 0.8)	(5.3, 7.3)
3.867	1.0	2.0	4.0	2.0	(0.3, 0.3)	(0.5, 1.7)	(1.1, 4.8)	(0.1, -)	(-, 0.5)	(1.0, 1.7)	(0.7, 0.8)	(5.3, 7.4)
3.871	1.0	2.0	4.0	2.0	(0.4, 0.3)	(0.2, 1.7)	(0.5, 4.8)	(0.4, -)	(-, 0.5)	(0.6, 1.5)	(0.7, 0.8)	(5.1, 7.4)
4.008	1.0	2.0	4.0	2.0	(0.2, 0.1)	(0.4, 1.7)	(1.0, 4.8)	(0.3, -)	(-, 0.5)	(2.8, 0.7)	(0.7, 0.8)	(5.9, 7.2)
4.129	1.0	2.0	4.0	2.0	(0.2, 0.4)	(0.4, 1.7)	(0.6, 4.8)	(0.2, -)	(-, 0.5)	(0.8, 1.3)	(0.7, 0.8)	(5.2, 7.3)
4.158	1.0	2.0	4.0	2.0	(0.2, 0.1)	(0.4, 1.7)	(0.3, 4.8)	(0.5, -)	(-, 0.5)	(0.6, 0.8)	(0.7, 0.8)	(5.1, 7.2)
4.178	1.0	2.0	4.0	2.0	(0.5, 0.3)	(0.1, 1.7)	(1.6, 4.8)	(0.1, -)	(-, 0.5)	(0.6, 0.8)	(0.7, 0.8)	(5.4, 7.2)
4.189	1.0	2.0	4.0	2.0	(0.3, 0.3)	(0.3, 1.7)	(0.8, 4.8)	(0.2, -)	(-, 0.5)	(0.6, 1.0)	(0.7, 0.8)	(5.2, 7.3)
4.199	1.0	2.0	4.0	2.0	(0.2, 0.2)	(0.6, 1.7)	(0.3, 4.8)	(0.1, -)	(-, 0.5)	(1.1, 0.9)	(0.7, 0.8)	(5.2, 7.3)
4.209	1.0	2.0	4.0	2.0	(0.2, 0.3)	(0.6, 1.7)	(0.9, 4.8)	(0.7, -)	(-, 0.5)	(0.7, 0.9)	(0.7, 0.8)	(5.3, 7.3)
4.219	1.0	2.0	4.0	2.0	(0.3, 0.2)	(0.2, 1.7)	(0.6, 4.8)	(0.8, -)	(-, 0.5)	(1.1, 1.2)	(0.7, 0.8)	(5.3, 7.3)
4.226	1.0	2.0	4.0	2.0	(0.2, 0.2)	(0.7, 1.7)	(0.6, 4.8)	(0.5, -)	(-, 0.5)	(1.9, 0.5)	(0.7, 0.8)	(5.5, 7.2)
4.236	1.0	2.0	4.0	2.0	(0.3, 0.2)	(0.3, 1.7)	(1.0, 4.8)	(0.4, -)	(-, 0.5)	(1.0, 0.4)	(0.7, 0.8)	(5.3, 7.2)
4.244	1.0	2.0	4.0	2.0	(0.3, 0.2)	(0.2, 1.7)	(3.4, 4.8)	(0.6, -)	(-, 0.5)	(0.8, 1.0)	(0.7, 0.8)	(6.2, 7.3)
4.258	1.0	2.0	4.0	2.0	(0.5, 0.2)	(0.3, 1.7)	(1.0, 4.8)	(0.4, -)	(-, 0.5)	(1.3, 2.2)	(0.7, 0.8)	(5.4, 7.5)
4.267	1.0	2.0	4.0	2.0	(0.3, 0.2)	(0.7, 1.7)	(0.9, 4.8)	(0.1, -)	(-, 0.5)	(1.2, 1.7)	(0.7, 0.8)	(5.3, 7.4)
4.278	1.0	2.0	4.0	2.0	(0.3, 0.2)	(1.4, 1.7)	(0.8, 4.8)	(0.1, -)	(-, 0.5)	(0.4, 0.1)	(0.7, 0.8)	(5.3, 7.2)
4.288	1.0	2.0	4.0	2.0	(0.3, 0.1)	(1.0, 1.7)	(3.0, 4.8)	(0.6, -)	(-, 0.5)	(1.0, 0.8)	(0.7, 0.8)	(6.1, 7.2)
4.312	1.0	2.0	4.0	2.0	(0.2, 0.3)	(0.8, 1.7)	(0.4, 4.8)	(0.6, -)	(-, 0.5)	(0.9, 0.4)	(0.7, 0.8)	(5.2, 7.2)
4.338	1.0	2.0	4.0	2.0	(0.3, 0.2)	(0.8, 1.7)	(1.1, 4.8)	(0.6, -)	(-, 0.5)	(0.9, 1.2)	(0.7, 0.8)	(5.3, 7.3)
4.358	1.0	2.0	4.0	2.0	(0.5, 0.2)	(0.9, 1.7)	(0.5, 4.8)	(0.2, -)	(-, 0.5)	(2.9, 1.0)	(0.7, 0.8)	(5.9, 7.3)
4.378	1.0	2.0	4.0	2.0	(0.4, 0.2)	(0.6, 1.7)	(0.6, 4.8)	(0.1, -)	(-, 0.5)	(1.2, 1.4)	(0.7, 0.8)	(5.3, 7.3)
4.397	1.0	2.0	4.0	2.0	(0.2, 0.1)	(0.9, 1.7)	(0.7, 4.8)	(0.8, -)	(-, 0.5)	(1.8, 0.3)	(0.7, 0.8)	(5.5, 7.2)
4.416	1.0	2.0	4.0	2.0	(0.2, 0.2)	(0.5, 1.7)	(2.3, 4.8)	(0.2, -)	(-, 0.5)	(1.3, 1.0)	(0.7, 0.8)	(5.7, 7.3)
4.437	1.0	2.0	4.0	2.0	(0.2, 0.2)	(0.9, 1.7)	(0.1, 4.8)	(0.8, -)	(-, 0.5)	(1.3, 0.5)	(0.7, 0.8)	(5.4, 7.2)
4.467	1.0	2.0	4.0	2.0	(0.3, 0.2)	(1.5, 1.7)	(3.1, 4.8)	(1.0, -)	(-, 0.5)	(0.7, 0.4)	(0.7, 0.8)	(6.2, 7.2)
4.527	1.0	2.0	4.0	2.0	(0.4, 0.1)	(3.2, 1.7)	(0.1, 4.8)	(0.1, -)	(-, 0.5)	(1.1, 0.7)	(0.7, 0.8)	(6.1, 7.2)
4.600	1.0	2.0	4.0	2.0	(0.4, 0.3)	(1.3, 1.7)	(1.4, 4.8)	(0.7, -)	(-, 0.5)	(1.4, 1.0)	(0.7, 0.8)	(5.6, 7.3)
4.615	1.0	2.0	4.0	2.0	(0.3, 0.2)	(1.3, 1.7)	(2.3, 4.8)	(2.0, -)	(-, 0.5)	(1.8, 1.2)	(0.7, 0.8)	(6.3, 7.3)
4.630	1.0	2.0	4.0	2.0	(0.3, 0.2)	(1.0, 1.7)	(0.3, 4.8)	(0.2, -)	(-, 0.5)	(0.1, 0.5)	(0.7, 0.8)	(5.2, 7.2)
4.643	1.0	2.0	4.0	2.0	(0.3, 0.3)	(0.8, 1.7)	(1.6, 4.8)	(0.6, -)	(-, 0.5)	(1.9, 1.3)	(0.7, 0.8)	(5.7, 7.3)
4.664	1.0	2.0	4.0	2.0	(0.3, 0.2)	(1.4, 1.7)	(0.9, 4.8)	(1.1, -)	(-, 0.5)	(0.5, 1.2)	(0.7, 0.8)	(5.5, 7.3)
4.684	1.0	2.0	4.0	2.0	(0.4, 0.3)	(0.7, 1.7)	(1.1, 4.8)	(0.5, -)	(-, 0.5)	(1.3, 0.8)	(0.7, 0.8)	(5.4, 7.2)
4.701	1.0	2.0	4.0	2.0	(0.3, 0.2)	(1.0, 1.7)	(1.8, 4.8)	(0.4, -)	(-, 0.5)	(1.8, 1.5)	(0.7, 0.8)	(5.8, 7.4)

6 Summary

We have measured the Born cross sections of two light hadron channels $e^+e^- \rightarrow \omega\pi^0$ and $\omega\eta$ using data samples collected at BESIII from $\sqrt{s} = 3.773$ to 4.701 GeV. A power-law function proportional to s^{-n} can describe both line shapes well. No obvious $\psi(4160)$, $Y(4230)$, $Y(4360)$, $\psi(4415)$, or $Y(4660)$ signal is found in the line shapes of $e^+e^- \rightarrow \omega\pi^0$ and $\omega\eta$. This indicates a relatively small branching fraction for these resonances into the $\omega\pi^0$ and $\omega\eta$ final states. More exploration of light hadron decay modes will be essential for a further understanding of the charmonium(-like) states.

Acknowledgments

The BESIII collaboration thanks the staff of BEPCII and the IHEP computing center for their strong support. This work is supported in part by National Key R&D Program of China under Contracts Nos. 2020YFA0406300, 2020YFA0406400; National Natural Science Foundation of China (NSFC) under Contracts Nos. 11875115, 11905179, 11625523, 11635010, 11735014, 11822506, 11835012, 11935015, 11935016, 11935018, 11961141012, 12022510, 12025502, 12035009, 12035013, 12061131003; the Chinese Academy of Sciences (CAS) Large-Scale Scientific Facility Program; Joint Large-Scale Scientific Facility Funds of the NSFC and CAS under Contracts Nos. U1732263, U1832207, U2032110; CAS Key Research Program of Frontier Sciences under Contract No. QYZDJ-SSW-SLH040; 100 Talents Program of CAS; INPAC and Shanghai Key Laboratory for Particle Physics and Cosmology; ERC under Contract No. 758462; European Union Horizon 2020 research and innovation programme under Contract No. Marie Skłodowska-Curie grant agreement No 894790; German Research Foundation DFG under Contracts Nos. 443159800, Collaborative Research Center CRC 1044, GRK 214; Istituto Nazionale di Fisica Nucleare, Italy; Ministry of Development of Turkey under Contract No. DPT2006K-120470; National Science and Technology fund; Olle Engkvist Foundation under Contract No. 200-0605; STFC (United Kingdom); The Knut and Alice Wallenberg Foundation (Sweden) under Contract No. 2016.0157; The Royal Society, UK under Contracts Nos. DH140054, DH160214; The Swedish Research Council; U. S. Department of Energy under Contracts Nos. DE-FG02-05ER41374, DE-SC-0012069.

References

- [1] Particle Data Group, *Review of Particle Physics*, [*PTEP* **2020** \(2020\) 083C01](#).
- [2] N. Brambilla *et al.*, *Heavy quarkonium: progress, puzzles, and opportunities*, [*Eur. Phys. J. C* **71** \(2011\) 1534](#).
- [3] H. X. Chen, W. Chen, X. Liu, and S. L. Zhu, *The hidden-charm pentaquark and tetraquark states*, [*Phys. Rept.* **639** \(2016\) 1](#).
- [4] Y. R. Liu, H. X. Chen, W. Chen, X. Liu and S. L. Zhu, *Pentaquark and Tetraquark states*, [*Prog. Part. Nucl. Phys.* **107** \(2019\) 237](#).
- [5] Belle collaboration, *Observation of a Narrow Charmoniumlike State in Exclusive $B^\pm \rightarrow K^\pm \pi^+ \pi^- J/\psi$ Decays*, [*Phys. Rev. Lett.* **91** \(2003\) 262001](#).

- [6] Babar collaboration, *Observation of a Broad Structure in the $\pi^+\pi^-J/\psi$ Mass Spectrum around 4.26 GeV/c²*, *Phys. Rev. Lett.* **95** (2005) 142001.
- [7] BESIII collaboration, *Observation of a Charged Charmoniumlike Structure in $e^+e^- \rightarrow \pi^+\pi^-J/\psi$ at 4.26 GeV/c²*, *Phys. Rev. Lett.* **110** (2013) 252001.
- [8] Belle collaboration, *Study of $e^+e^- \rightarrow \pi^+\pi^-J/\psi$ and Observation of a Charged Charmoniumlike State at Belle*, *Phys. Rev. Lett.* **110** (2013) 252002.
- [9] CLEO collaboration, *Charmonium Decays of $Y(4260)$, $Y(4260)$, and $Y(4040)$* , *Phys. Rev. Lett.* **96** (2006) 162003.
- [10] Belle collaboration, *Measurement of the $e^+e^- \rightarrow \pi^+\pi^-J/\psi$ Cross Section Via Initial-State Radiation at Belle*, *Phys. Rev. Lett.* **99** (2007) 182004.
- [11] BaBar collaboration, *Evidence of a Broad Structure at an Invariant Mass of 4.32 GeV/c² in the Reaction $e^+e^- \rightarrow \pi^+\pi^-\psi(2S)$ Measured at BABAR*, *Phys. Rev. Lett.* **98** (2007) 212001.
- [12] Belle collaboration, *Observation of Two Resonant Structures in $e^+e^- \rightarrow \pi^+\pi^-\psi(2S)$ via Initial-State Radiation at Belle*, *Phys. Rev. Lett.* **99** (2007) 142002.
- [13] BESIII collaboration, *Precise Measurement of the $e^+e^- \rightarrow \pi^+\pi^-J/\psi$ Cross Section at Center-of-Mass Energies from 3.77 to 4.60 GeV*, *Phys. Rev. Lett.* **118** (2017) 092001.
- [14] BESIII collaboration, *Cross section measurements of $e^+e^- \rightarrow \omega\chi_{c0}$ from $\sqrt{s}=4.178$ to 4.278 GeV*, *Phys. Rev. D* **99** (2019) 091103.
- [15] BESIII collaboration, *Evidence of Two Resonant Structures in $e^+e^- \rightarrow \pi^+\pi^-h_c$* , *Phys. Rev. Lett.* **118** (2017) 092002.
- [16] BESIII collaboration, *Measurement of $e^+e^- \rightarrow \pi^+\pi^-\psi(3686)$ from 4.008 to 4.600 GeV and observation of a charged structure in the $\pi^\pm\psi(3686)$ mass spectrum*, *Phys. Rev. D* **96** (2017) 032004.
- [17] BESIII collaboration, *Observation of a Charged $(D\bar{D}^*)^\pm$ Mass Peak in $e^+e^- \rightarrow \pi D\bar{D}^*$ at $\sqrt{s}=4.26$ GeV*, *Phys. Rev. Lett.* **112** (2014) 022001.
- [18] BESIII collaboration, *Measurement of $e^+e^- \rightarrow K_S^0 K^\pm \pi^\mp \pi^0$ and $K_S^0 K^\pm \pi^\mp \eta$ at center-of-mass energies from 3.90 to 4.60 GeV*, *Phys. Rev. D* **99** (2019) 012003.
- [19] BESIII collaboration, *First measurement of $e^+e^- \rightarrow pK_S^0 \bar{n}K^- + c.c.$ above open charm threshold*, *Phys. Rev. D* **98** (2018) 032014.
- [20] BESIII collaboration, *Cross section measurements of $e^+e^- \rightarrow p\bar{p}\pi^0$ at center-of-mass energies between 4.008 and 4.600 GeV*, *Phys. Lett. B* **771** (2017) 45.
- [21] BESIII collaboration, *Cross section measurement of $e^+e^- \rightarrow p\bar{p}\eta$ and $e^+e^- \rightarrow p\bar{p}\omega$ at center-of-mass energies between 3.773 GeV and 4.6 GeV*, *Phys. Rev. D* **104** (2021) 092008.
- [22] BESIII collaboration, *Design and construction of the BESIII detector*, *Nucl. Instrum. Meth. A* **614** (2010) 345.
- [23] C. H. Yu et al., *BEPCII Performance and Beam Dynamics Studies on Luminosity*, Proceedings of IPAC2016, Busan, Korea, 2016, [doi:10.18429/JACoW-IPAC2016-TUYA01](https://doi.org/10.18429/JACoW-IPAC2016-TUYA01).
- [24] X. Li et al., *Study of MRPC technology for BESIII endcap-TOF upgrade*, *Radiat. Detect. Technol. Methods* **1** (2017) 13; Y. X. Guo et al., *The study of time calibration for upgraded end cap TOF of BESIII*, *Radiat. Detect. Technol. Methods* **1** (2017) 15; P. Cao et al., *Design and construction of the new BESIII endcap Time-of-Flight system with MRPC Technology*, *Nucl. Instrum. Meth. A* **953** (2020) 163053.

- [25] GEANT4 collaboration, *GEANT4—a simulation toolkit*, *Nucl. Instrum. Meth. A* **506** (2003) 250.
- [26] S. Jadach, B. F. L. Ward and Z. Was, *Coherent exclusive exponentiation for precision Monte Carlo calculations*, *Phys. Rev. D* **63** (2001) 113009; *The precision Monte Carlo event generator KK for two-fermion final states in e^+e^- collisions*, *Comput. Phys. Commun.* **130** (2000) 260.
- [27] D. J. Lange, *The EvtGen particle decay simulation package*, *Nucl. Instrum. Meth. A* **462** (2001) 152; R. G. Ping, *Event generators at BESIII*, *Chin. Phys. C* **32** (2008) 599.
- [28] J. C. Chen, G. S. Huang, X. R. Qi, D. H. Zhang and Y. S. Zhu, *Event generator for J/ψ and $\psi(2S)$ decay*, *Phys. Rev. D* **62** (2000) 034003; R. L. Yang, R. G. Ping and H. Chen, *Tuning and Validation of the Lundcharm Model with J/ψ Decays*, *Chin. Phys. Lett.* **31** (2014) 061301.
- [29] E. Richter-Was, *QED bremsstrahlung in semileptonic B and leptonic τ decays*, *Phys. Lett. B* **303** (1993) 163.
- [30] X. Y. Zhou, S. X. Du, G. Li and C. P. Shen, *TopoAna: A generic tool for the event type analysis of inclusive Monte-Carlo samples in high energy physics experiments*, *Comput. Phys. Commun.* **258** (2021), 107540.
- [31] BESIII collaboration, *Cross section measurement of $e^+e^- \rightarrow \eta' J/\psi$ from $\sqrt{s}=4.178$ to 4.600 GeV*, *Phys. Rev. D* **101** (2020) 012008.
- [32] BESIII collaboration, *Precision measurement of the integrated luminosity of the data taken by BESIII at center-of-mass energies between 3.810 GeV and 4.600 GeV*, *Chin. Phys. C* **39** (2015) 093001.
- [33] BESIII collaboration, *Search for new decay modes of the $\psi_2(3823)$ and the process $e^+e^- \rightarrow \pi^0\pi^0\psi_2(3823)$* , *Phys. Rev. D* **103** (2021) L091102.
- [34] BESIII collaboration, *Study of χ_{cJ} radiative decays into a vector meson*, *Phys. Rev. D* **83** (2011) 112005.
- [35] BESIII collaboration, *Search for hadronic transition $\chi_{cJ} \rightarrow \eta_c \pi^+ \pi^-$ and observation of $\chi_{cJ} \rightarrow K \bar{K} \pi \pi$* , *Phys. Rev. D* **87** (2013) 012002.

The BESIII collaboration

M. Ablikim¹, M. N. Achasov^{10,b}, P. Adlarson⁶⁸, S. Ahmed¹⁴, M. Albrecht⁴, R. Aliberti²⁸, A. Amoroso^{67A,67C}, M. R. An³², Q. An^{50,64}, X. H. Bai⁵⁸, Y. Bai⁴⁹, O. Bakina²⁹, R. Baldini Ferroli^{23A}, I. Balossino^{24A,1}, Y. Ban^{39,h}, V. Batozskaya^{1,37}, D. Becker²⁸, K. Begzsuren²⁶, N. Berger²⁸, M. Bertani^{23A}, D. Bettoni^{24A}, F. Bianchi^{67A,67C}, J. Bloms⁶¹, A. Bortone^{67A,67C}, I. Boyko²⁹, R. A. Briere⁵, H. Cai⁶⁹, X. Cai^{1,50}, A. Calcaterra^{23A}, G. F. Cao^{1,55}, N. Cao^{1,55}, S. A. Cetin^{54A}, J. F. Chang^{1,50}, W. L. Chang^{1,55}, G. Chelkov^{29,a}, C. Chen³⁶, G. Chen¹, H. S. Chen^{1,55}, M. L. Chen^{1,50}, S. J. Chen³⁵, T. Chen¹, X. R. Chen²⁵, X. T. Chen¹, Y. B. Chen^{1,50}, Z. J. Chen^{20,i}, W. S. Cheng^{67C}, G. Cibinetto^{24A}, F. Cossio^{67C}, J. J. Cui⁴², X. F. Cui³⁶, H. L. Dai^{1,50}, J. P. Dai⁷¹, X. C. Dai^{1,55}, A. Dbeyssi¹⁴, R. E. de Boer⁴, D. Dedovich²⁹, Z. Y. Deng¹, A. Denig²⁸, I. Denysenko²⁹, M. Destefanis^{67A,67C}, F. De Mori^{67A,67C}, Y. Ding³³, C. Dong³⁶, J. Dong^{1,50}, L. Y. Dong^{1,55}, M. Y. Dong¹, X. Dong⁶⁹, S. X. Du⁷³, P. Egorov^{29,a}, Y. L. Fan⁶⁹, J. Fang^{1,50}, S. S. Fang^{1,55}, Y. Fang¹, R. Farinelli^{24A}, L. Fava^{67B,67C}, F. Feldbauer⁴, G. Felici^{23A}, C. Q. Feng^{50,64}, J. H. Feng⁵¹, M. Fritsch⁴, C. D. Fu¹, Y. N. Gao^{39,h}, Yang Gao^{50,64}, I. Garzia^{24A,24B}, P. T. Ge⁶⁹, C. Geng⁵¹, E. M. Gersabeck⁵⁹, A. Gilman⁶², K. Goetzen¹¹, L. Gong³³, W. X. Gong^{1,50}, W. Gradl²⁸, M. Greco^{67A,67C}, M. H. Gu^{1,50}, C. Y. Guan^{1,55}, A. Q. Guo²⁵, A. Q. Guo²², L. B. Guo³⁴, R. P. Guo⁴¹, Y. P. Guo^{9,g}, A. Guskov^{29,a}, T. T. Han⁴², W. Y. Han³², X. Q. Hao¹⁵, F. A. Harris⁵⁷, K. K. He⁴⁷, K. L. He^{1,55}, F. H. Heinsius⁴, C. H. Heinz²⁸, Y. K. Heng¹, C. Herold⁵², M. Himmelreich^{11,e}, T. Holtmann⁴, G. Y. Hou^{1,55}, Y. R. Hou⁵⁵, Z. L. Hou¹, H. M. Hu^{1,55}, J. F. Hu^{48,j}, T. Hu¹, Y. Hu¹, G. S. Huang^{50,64}, L. Q. Huang⁶⁵, X. T. Huang⁴², Y. P. Huang¹, Z. Huang^{39,h}, T. Hussain⁶⁶, N. Hüskens^{22,28}, W. Ikegami Andersson⁶⁸, W. Imoehl²², M. Irshad^{50,64}, S. Jaeger⁴, S. Janchiv²⁶, Q. Ji¹, Q. P. Ji¹⁵, X. B. Ji^{1,55}, X. L. Ji^{1,50}, Y. Y. Ji⁴², H. B. Jiang⁴², S. S. Jiang³², X. S. Jiang¹, J. B. Jiao⁴², Z. Jiao¹⁸, S. Jin³⁵, Y. Jin⁵⁸, M. Q. Jing^{1,55}, T. Johansson⁶⁸, N. Kalantar-Nayestanaki⁵⁶, X. S. Kang³³, R. Kappert⁵⁶, M. Kavatsyuk⁵⁶, B. C. Ke⁷³, I. K. Keshk⁴, A. Khoukaz⁶¹, P. Kiese²⁸, R. Kiuchi¹, R. Kliemt¹¹, L. Koch³⁰, O. B. Kolcu^{54A}, B. Kopf⁴, M. Kuemmel⁴, M. Kuessner⁴, A. Kupsc^{37,68}, M. G. Kurth^{1,55}, W. Kühn³⁰, J. J. Lane⁵⁹, J. S. Lange³⁰, P. Larin¹⁴, A. Lavania²¹, L. Lavezzi^{67A,67C}, Z. H. Lei^{50,64}, H. Leithoff²⁸, M. Lellmann²⁸, T. Lenz²⁸, C. Li⁴⁰, C. Li³⁶, C. H. Li³², Cheng Li^{50,64}, D. M. Li⁷³, F. Li^{1,50}, G. Li¹, H. Li^{50,64}, H. Li⁴⁴, H. B. Li^{1,55}, H. J. Li¹⁵, H. N. Li^{48,j}, J. L. Li⁴², J. Q. Li⁴, J. S. Li⁵¹, Ke Li¹, L. J. Li¹, L. K. Li¹, Lei Li³, M. H. Li³⁶, P. R. Li^{31,k,l}, S. X. Li⁹, S. Y. Li⁵³, T. Li⁴², W. D. Li^{1,55}, W. G. Li¹, X. H. Li^{50,64}, X. L. Li⁴², Xiaoyu Li^{1,55}, Z. Y. Li⁵¹, H. Liang^{1,55}, H. Liang^{50,64}, H. Liang²⁷, Y. F. Liang⁴⁶, Y. T. Liang²⁵, G. R. Liao¹², L. Z. Liao^{1,55}, J. Libby²¹, A. Limphirat⁵², C. X. Lin⁵¹, D. X. Lin²⁵, T. Lin¹, B. J. Liu¹, C. X. Liu¹, D. Liu^{14,64}, F. H. Liu⁴⁵, Fang Liu¹, Feng Liu⁶, G. M. Liu^{48,j}, H. M. Liu^{1,55}, Huanhuan Liu¹, Huihui Liu¹⁶, J. B. Liu^{50,64}, J. L. Liu⁶⁵, J. Y. Liu^{1,55}, K. Liu¹, K. Y. Liu³³, Ke Liu¹⁷, L. Liu^{50,64}, M. H. Liu^{9,g}, P. L. Liu¹, Q. Liu⁵⁵, S. B. Liu^{50,64}, T. Liu^{1,55}, T. Liu^{9,g}, W. M. Liu^{50,64}, X. Liu^{31,k,l}, Y. Liu^{31,k,l}, Y. B. Liu³⁶, Z. A. Liu¹, Z. Q. Liu⁴², X. C. Lou¹, F. X. Lu⁵¹, H. J. Lu¹⁸, J. D. Lu^{1,55}, J. G. Lu^{1,50}, X. L. Lu¹, Y. Lu¹, Y. P. Lu^{1,50}, Z. H. Lu¹, C. L. Luo³⁴, M. X. Luo⁷², T. Luo^{9,g}, X. L. Luo^{1,50}, X. R. Lyu⁵⁵, Y. F. Lyu³⁶, F. C. Ma³³, H. L. Ma¹, L. L. Ma⁴², M. M. Ma^{1,55}, Q. M. Ma¹, R. Q. Ma^{1,55}, R. T. Ma⁵⁵, X. X. Ma^{1,55}, X. Y. Ma^{1,50}, Y. Ma^{39,h}, F. E. Maas¹⁴, M. Maggiora^{67A,67C}, S. Maldaner⁴, S. Malde⁶², Q. A. Malik⁶⁶, A. Mangoni^{23B}, Y. J. Mao^{39,h}, Z. P. Mao¹, S. Marcello^{67A,67C}, Z. X. Meng⁵⁸, J. G. Messchendorp^{56,d}, G. Mezzadri^{24A,1}, H. Miao¹, T. J. Min³⁵, R. E. Mitchell²², X. H. Mo¹, N. Yu. Muchnoi^{10,b}, H. Muramatsu⁶⁰, S. Nakhoul^{11,e}, Y. Nefedov²⁹, F. Nerling^{11,e}, I. B. Nikolaev^{10,b}, Z. Ning^{1,50}, S. Nisar^{8,m}, S. L. Olsen⁵⁵, Q. Ouyang¹, S. Pacetti^{23B,23C}, X. Pan^{9,g}, Y. Pan⁵⁹, A. Pathak¹, A. Pathak²⁷, P. Patteri^{23A}, M. Pelzaeus⁴, H. P. Peng^{50,64}, K. Peters^{11,e}, J. Pettersson⁶⁸, J. L. Ping³⁴, R. G. Ping^{1,55}, S. Plura²⁸, S. Pogodin²⁹, R. Poling⁶⁰, V. Prasad^{50,64}, H. Qi^{50,64}, H. R. Qi⁵³, M. Qi³⁵, T. Y. Qi^{9,g}, S. Qian^{1,50}, W. B. Qian⁵⁵, Z. Qian⁵¹, C. F. Qiao⁵⁵, J. J. Qin⁶⁵, L. Q. Qin¹², X. P. Qin^{9,g}, X. S. Qin⁴², Z. H. Qin^{1,50}, J. F. Qiu¹, S. Q. Qu³⁶, K. H. Rashid⁶⁶,

K. Ravindran²¹, C. F. Redmer²⁸, K. J. Ren³², A. Rivetti^{67C}, V. Rodin⁵⁶, M. Rolo^{67C}, G. Rong^{1,55}, Ch. Rosner¹⁴, M. Rump⁶¹, H. S. Sang⁶⁴, A. Sarantsev^{29,c}, Y. Schelhaas²⁸, C. Schnier⁴, K. Schoenning⁶⁸, M. Scodreggio^{24A,24B}, K. Y. Shan^{9,g}, W. Shan¹⁹, X. Y. Shan^{50,64}, J. F. Shangguan⁴⁷, L. G. Shao^{1,55}, M. Shao^{50,64}, C. P. Shen^{9,g}, H. F. Shen^{1,55}, X. Y. Shen^{1,55}, B.-A. Shi⁵⁵, H. C. Shi^{50,64}, R. S. Shi^{1,55}, X. Shi^{1,50}, X. D Shi^{50,64}, J. J. Song¹⁵, W. M. Song^{1,27}, Y. X. Song^{39,h}, S. Sosio^{67A,67C}, S. Spataro^{67A,67C}, F. Stieler²⁸, K. X. Su⁶⁹, P. P. Su⁴⁷, Y.-J. Su⁵⁵, G. X. Sun¹, H. K. Sun¹, J. F. Sun¹⁵, L. Sun⁶⁹, S. S. Sun^{1,55}, T. Sun^{1,55}, W. Y. Sun²⁷, X. Sun^{20,i}, Y. J. Sun^{50,64}, Y. Z. Sun¹, Z. T. Sun⁴², Y. H. Tan⁶⁹, Y. X. Tan^{50,64}, C. J. Tang⁴⁶, G. Y. Tang¹, J. Tang⁵¹, L. Y. Tao⁶⁵, Q. T. Tao^{20,i}, J. X. Teng^{50,64}, V. Thoren⁶⁸, W. H. Tian⁴⁴, Y. T. Tian²⁵, I. Uman^{54B}, B. Wang¹, D. Y. Wang^{39,h}, F. Wang⁶⁵, H. J. Wang^{31,k,l}, H. P. Wang^{1,55}, K. Wang^{1,50}, L. L. Wang¹, M. Wang⁴², M. Z. Wang^{39,h}, Meng Wang^{1,55}, S. Wang^{9,g}, T. J. Wang³⁶, W. Wang⁵¹, W. H. Wang⁶⁹, W. P. Wang^{50,64}, X. Wang^{39,h}, X. F. Wang^{31,k,l}, X. L. Wang^{9,g}, Y. D. Wang³⁸, Y. F. Wang¹, Y. Q. Wang¹, Y. Y. Wang^{31,k,l}, Ying Wang⁵¹, Z. Wang^{1,50}, Z. Y. Wang¹, Ziyi Wang⁵⁵, Zongyuan Wang^{1,55}, D. H. Wei¹², F. Weidner⁶¹, S. P. Wen¹, D. J. White⁵⁹, U. Wiedner⁴, G. Wilkinson⁶², M. Wolke⁶⁸, L. Wollenberg⁴, J. F. Wu^{1,55}, L. H. Wu¹, L. J. Wu^{1,55}, X. Wu^{9,g}, X. H. Wu²⁷, Z. Wu^{1,50}, L. Xia^{50,64}, T. Xiang^{39,h}, H. Xiao^{9,g}, S. Y. Xiao¹, Y. L. Xiao^{9,g}, Z. J. Xiao³⁴, X. H. Xie^{39,h}, Y. G. Xie^{1,50}, Y. H. Xie⁶, T. Y. Xing^{1,55}, C. F. Xu¹, C. J. Xu⁵¹, G. F. Xu¹, Q. J. Xu¹³, S. Y. Xu⁶³, W. Xu^{1,55}, X. P. Xu⁴⁷, Y. C. Xu⁵⁵, F. Yan^{9,g}, L. Yan^{9,g}, W. B. Yan^{50,64}, W. C. Yan⁷³, H. J. Yang^{43,f}, H. X. Yang¹, L. Yang⁴⁴, S. L. Yang⁵⁵, Y. X. Yang¹², Y. X. Yang^{1,55}, Yifan Yang^{1,55}, Zhi Yang²⁵, M. Ye^{1,50}, M. H. Ye⁷, J. H. Yin¹, Z. Y. You⁵¹, B. X. Yu¹, C. X. Yu³⁶, G. Yu^{1,55}, J. S. Yu^{20,i}, T. Yu⁶⁵, C. Z. Yuan^{1,55}, L. Yuan², S. C. Yuan¹, X. Q. Yuan¹, Y. Yuan¹, Z. Y. Yuan⁵¹, C. X. Yue³², A. A. Zafar⁶⁶, X. Zeng Zeng⁶, Y. Zeng^{20,i}, A. Q. Zhang¹, B. L. Zhang¹, B. X. Zhang¹, G. Y. Zhang¹⁵, H. Zhang⁶⁴, H. H. Zhang⁵¹, H. H. Zhang²⁷, H. Y. Zhang^{1,50}, J. L. Zhang⁷⁰, J. Q. Zhang³⁴, J. W. Zhang¹, J. Y. Zhang¹, J. Z. Zhang^{1,55}, Jianyu Zhang^{1,55}, Jiawei Zhang^{1,55}, L. M. Zhang⁵³, L. Q. Zhang⁵¹, Lei Zhang³⁵, P. Zhang¹, Shulei Zhang^{20,i}, X. D. Zhang³⁸, X. M. Zhang¹, X. Y. Zhang⁴², X. Y. Zhang⁴⁷, Y. Zhang⁶², Y. T. Zhang⁷³, Y. H. Zhang^{1,50}, Yan Zhang^{50,64}, Yao Zhang¹, Z. H. Zhang¹, Z. Y. Zhang³⁶, Z. Y. Zhang⁶⁹, G. Zhao¹, J. Zhao³², J. Y. Zhao^{1,55}, J. Z. Zhao^{1,50}, Lei Zhao^{50,64}, Ling Zhao¹, M. G. Zhao³⁶, Q. Zhao¹, S. J. Zhao⁷³, Y. B. Zhao^{1,50}, Y. X. Zhao²⁵, Z. G. Zhao^{50,64}, A. Zhemchugov^{29,a}, B. Zheng⁶⁵, J. P. Zheng^{1,50}, Y. H. Zheng⁵⁵, B. Zhong³⁴, C. Zhong⁶⁵, L. P. Zhou^{1,55}, Q. Zhou^{1,55}, X. Zhou⁶⁹, X. K. Zhou⁵⁵, X. R. Zhou^{50,64}, X. Y. Zhou³², Y. Z. Zhou^{9,g}, A. N. Zhu^{1,55}, J. Zhu³⁶, K. Zhu¹, K. J. Zhu¹, S. H. Zhu⁶³, T. J. Zhu⁷⁰, W. J. Zhu^{9,g}, W. J. Zhu³⁶, Y. C. Zhu^{50,64}, Z. A. Zhu^{1,55}, B. S. Zou¹, J. H. Zou¹

¹ *Institute of High Energy Physics, Beijing 100049, People's Republic of China*

² *Beihang University, Beijing 100191, People's Republic of China*

³ *Beijing Institute of Petrochemical Technology, Beijing 102617, People's Republic of China*

⁴ *Bochum Ruhr-University, D-44780 Bochum, Germany*

⁵ *Carnegie Mellon University, Pittsburgh, Pennsylvania 15213, USA*

⁶ *Central China Normal University, Wuhan 430079, People's Republic of China*

⁷ *China Center of Advanced Science and Technology, Beijing 100190, People's Republic of China*

⁸ *COMSATS University Islamabad, Lahore Campus, Defence Road, Off Raiwind Road, 54000 Lahore, Pakistan*

⁹ *Fudan University, Shanghai 200443, People's Republic of China*

¹⁰ *G.I. Budker Institute of Nuclear Physics SB RAS (BINP), Novosibirsk 630090, Russia*

¹¹ *GSI Helmholtzcentre for Heavy Ion Research GmbH, D-64291 Darmstadt, Germany*

¹² *Guangxi Normal University, Guilin 541004, People's Republic of China*

¹³ *Hangzhou Normal University, Hangzhou 310036, People's Republic of China*

¹⁴ *Helmholtz Institute Mainz, Staudinger Weg 18, D-55099 Mainz, Germany*

¹⁵ *Henan Normal University, Xinxiang 453007, People's Republic of China*

- ¹⁶ *Henan University of Science and Technology, Luoyang 471003, People's Republic of China*
- ¹⁷ *Henan University of Technology, Zhengzhou 450001, People's Republic of China*
- ¹⁸ *Huangshan College, Huangshan 245000, People's Republic of China*
- ¹⁹ *Hunan Normal University, Changsha 410081, People's Republic of China*
- ²⁰ *Hunan University, Changsha 410082, People's Republic of China*
- ²¹ *Indian Institute of Technology Madras, Chennai 600036, India*
- ²² *Indiana University, Bloomington, Indiana 47405, USA*
- ²³ *(A)INFN Laboratori Nazionali di Frascati, I-00044, Frascati, Italy; (B)INFN Sezione di Perugia, I-06100, Perugia, Italy; (C)University of Perugia, I-06100, Perugia, Italy*
- ²⁴ *(A)INFN Sezione di Ferrara, I-44122, Ferrara, Italy; (B)University of Ferrara, I-44122, Ferrara, Italy*
- ²⁵ *Institute of Modern Physics, Lanzhou 730000, People's Republic of China*
- ²⁶ *Institute of Physics and Technology, Peace Ave. 54B, Ulaanbaatar 13330, Mongolia*
- ²⁷ *Jilin University, Changchun 130012, People's Republic of China*
- ²⁸ *Johannes Gutenberg University of Mainz, Johann-Joachim-Becher-Weg 45, D-55099 Mainz, Germany*
- ²⁹ *Joint Institute for Nuclear Research, 141980 Dubna, Moscow region, Russia*
- ³⁰ *Justus-Liebig-Universitaet Giessen, II. Physikalisches Institut, Heinrich-Buff-Ring 16, D-35392 Giessen, Germany*
- ³¹ *Lanzhou University, Lanzhou 730000, People's Republic of China*
- ³² *Liaoning Normal University, Dalian 116029, People's Republic of China*
- ³³ *Liaoning University, Shenyang 110036, People's Republic of China*
- ³⁴ *Nanjing Normal University, Nanjing 210023, People's Republic of China*
- ³⁵ *Nanjing University, Nanjing 210093, People's Republic of China*
- ³⁶ *Nankai University, Tianjin 300071, People's Republic of China*
- ³⁷ *National Centre for Nuclear Research, Warsaw 02-093, Poland*
- ³⁸ *North China Electric Power University, Beijing 102206, People's Republic of China*
- ³⁹ *Peking University, Beijing 100871, People's Republic of China*
- ⁴⁰ *Qufu Normal University, Qufu 273165, People's Republic of China*
- ⁴¹ *Shandong Normal University, Jinan 250014, People's Republic of China*
- ⁴² *Shandong University, Jinan 250100, People's Republic of China*
- ⁴³ *Shanghai Jiao Tong University, Shanghai 200240, People's Republic of China*
- ⁴⁴ *Shanxi Normal University, Linfen 041004, People's Republic of China*
- ⁴⁵ *Shanxi University, Taiyuan 030006, People's Republic of China*
- ⁴⁶ *Sichuan University, Chengdu 610064, People's Republic of China*
- ⁴⁷ *Soochow University, Suzhou 215006, People's Republic of China*
- ⁴⁸ *South China Normal University, Guangzhou 510006, People's Republic of China*
- ⁴⁹ *Southeast University, Nanjing 211100, People's Republic of China*
- ⁵⁰ *State Key Laboratory of Particle Detection and Electronics, Beijing 100049, Hefei 230026, People's Republic of China*
- ⁵¹ *Sun Yat-Sen University, Guangzhou 510275, People's Republic of China*
- ⁵² *Suranaree University of Technology, University Avenue 111, Nakhon Ratchasima 30000, Thailand*
- ⁵³ *Tsinghua University, Beijing 100084, People's Republic of China*
- ⁵⁴ *(A)Istinye University, 34010, Istanbul, Turkey; (B)Near East University, Nicosia, North Cyprus, Mersin 10, Turkey*
- ⁵⁵ *University of Chinese Academy of Sciences, Beijing 100049, People's Republic of China*
- ⁵⁶ *University of Groningen, NL-9747 AA Groningen, The Netherlands*

- ⁵⁷ *University of Hawaii, Honolulu, Hawaii 96822, USA*
- ⁵⁸ *University of Jinan, Jinan 250022, People's Republic of China*
- ⁵⁹ *University of Manchester, Oxford Road, Manchester, M13 9PL, United Kingdom*
- ⁶⁰ *University of Minnesota, Minneapolis, Minnesota 55455, USA*
- ⁶¹ *University of Muenster, Wilhelm-Klemm-Str. 9, 48149 Muenster, Germany*
- ⁶² *University of Oxford, Keble Rd, Oxford, UK OX13RH*
- ⁶³ *University of Science and Technology Liaoning, Anshan 114051, People's Republic of China*
- ⁶⁴ *University of Science and Technology of China, Hefei 230026, People's Republic of China*
- ⁶⁵ *University of South China, Hengyang 421001, People's Republic of China*
- ⁶⁶ *University of the Punjab, Lahore-54590, Pakistan*
- ⁶⁷ *(A)University of Turin, I-10125, Turin, Italy; (B)University of Eastern Piedmont, I-15121, Alessandria, Italy; (C)INFN, I-10125, Turin, Italy*
- ⁶⁸ *Uppsala University, Box 516, SE-75120 Uppsala, Sweden*
- ⁶⁹ *Wuhan University, Wuhan 430072, People's Republic of China*
- ⁷⁰ *Xinyang Normal University, Xinyang 464000, People's Republic of China*
- ⁷¹ *Yunnan University, Kunming 650500, People's Republic of China*
- ⁷² *Zhejiang University, Hangzhou 310027, People's Republic of China*
- ⁷³ *Zhengzhou University, Zhengzhou 450001, People's Republic of China*
- ^a *Also at the Moscow Institute of Physics and Technology, Moscow 141700, Russia*
- ^b *Also at the Novosibirsk State University, Novosibirsk, 630090, Russia*
- ^c *Also at the NRC "Kurchatov Institute", PNPI, 188300, Gatchina, Russia*
- ^d *Currently at Istanbul Arel University, 34295 Istanbul, Turkey*
- ^e *Also at Goethe University Frankfurt, 60323 Frankfurt am Main, Germany*
- ^f *Also at Key Laboratory for Particle Physics, Astrophysics and Cosmology, Ministry of Education; Shanghai Key Laboratory for Particle Physics and Cosmology; Institute of Nuclear and Particle Physics, Shanghai 200240, People's Republic of China*
- ^g *Also at Key Laboratory of Nuclear Physics and Ion-beam Application (MOE) and Institute of Modern Physics, Fudan University, Shanghai 200443, People's Republic of China*
- ^h *Also at State Key Laboratory of Nuclear Physics and Technology, Peking University, Beijing 100871, People's Republic of China*
- ⁱ *Also at School of Physics and Electronics, Hunan University, Changsha 410082, China*
- ^j *Also at Guangdong Provincial Key Laboratory of Nuclear Science, Institute of Quantum Matter, South China Normal University, Guangzhou 510006, China*
- ^k *Also at Frontiers Science Center for Rare Isotopes, Lanzhou University, Lanzhou 730000, People's Republic of China*
- ^l *Also at Lanzhou Center for Theoretical Physics, Lanzhou University, Lanzhou 730000, People's Republic of China*
- ^m *Also at the Department of Mathematical Sciences, IBA, Karachi, Pakistan*